Available online at www.sciencedirect.com
SCIENCE DIRECT®
Journal of Power Sources 115 (2003) 90–100
JOURNAL OF POWER SOURCES
www.elsevier.com/locate/jpowsour

Multi-gas transportation and electrochemical performance of a polymer electrolyte fuel cell with complex flow channels

Pei-Wen Li*, Laura Schaefer, Qing-Ming Wang, Tao Zhang, Minking K. Chyu

Department of Mechanical Engineering, Benedum Engineering Hall, University of Pittsburgh, Pittsburgh, PA 15261, USA

Received 20 November 2002; accepted 29 November 2002

Abstract

A three-dimensional (3D) numerical model associating the heat/mass transfer and the electrochemical reaction in a proton exchange membrane (PEM) fuel cell is developed in this study, and a miniaturized PEM fuel cell with complex flow channels is simulated. The numerical computation is based on the finite-volume method. Governing equations for flow and heat/mass transfer are coupled with the electrochemical reactions and are solved simultaneously. The latent heat from the condensation of water vapor in cathode channel, if any, is considered. The perimeters of the bipolar plates are also included in the computational domain to account for their heat conduction effect. The miniaturized PEM fuel cell has a membrane electrode assembly (MEA) sandwiched by two brass bipolar plates etched with a number of winding gas channels with a flow area of 250 μm × 250 μm. The influence of anode gas humidity on the performance of the fuel cell is investigated through model prediction. Finally, field details of velocity, mass fraction and electromotive force are illustrated and discussed.
© 2003 Published by Elsevier Science B.V.

Keywords: PEM fuel cell; 3D numerical model; Complex flow channels; Heat/mass transfer

1. Introduction

Proton exchange membrane (PEM) fuel cells operate at a low temperature (from room temperature to 90 °C) to convert chemical energy directly into electrical energy. Low emission of pollutants and high electricity conversion efficiency make this technology attractive, and it is currently being considered as one of the most promising candidates for stationary and automotive applications as a substitute of traditional power systems (i.e. thermoelectric power plants and internal combustion engines) [1–4].

A PEM fuel cell consists of three major components: an anode, typically featuring a platinum or platinum-containing catalyst; a thin, solid polymeric membrane which acts as the electrolyte; and a cathode, also platinum-catalyzed. The reactions in a PEM fuel cell fed with a hydrogen-containing anode gas (hydrogen with some amount of water vapor) and an oxygen-containing cathode gas (air) are:

$$H_2 \leftrightarrow 2H^+ + 2e^- \quad \text{(anode)} \tag{1}$$

$$2H^+ + 2e^- + \tfrac{1}{2}O_2 \leftrightarrow H_2O \quad \text{(cathode)} \tag{2}$$

$$H_2 + \tfrac{1}{2}O_2 \leftrightarrow H_2O \quad \text{(overall)} \tag{3}$$

From Nernst equation, the thereby induced electromotive force or electrical potential between the cathode and anode is a function of the temperature at the reaction site and the partial pressures of reactants and products as well:

$$E = \frac{-\Delta G_0}{2F} + \frac{RT}{2F} \ln\left(\frac{P_{H_2} P_{O_2}^{0.5}}{P_{H_2O}}\right) \tag{4}$$

where ΔG_0 is the standard Gibbs free energy change (high heat value) of the electrochemical reaction at temperature T; the P with the respective subscripts are the partial pressures of the corresponding reactants and products at the electrolyte/electrode interfaces; F the Faraday's constant; and R is the universal gas constant.

As typical component of a PEM fuel cell, a plate (made of high conductivity material) etched with winding grooves serving as gas channels, is shown in Fig. 1. Two such plates sandwiching a layer of membrane electrode assembly (MEA) on their grooved side can compose a single PEM fuel cell. Fuel is fed to the channels of the anode side, and in a similar way, air is fed to the channels of the cathode side. With many such single fuel cell units being laminated in series, a cell stack can be constructed. In practical terms, plates with channels etched on two sides are used to sandwich the MEA so as to construct a PEM fuel cell stack. Such a plate is referred to as a bipolar plate [1]. A detailed study of

* Corresponding author. Tel.: +1-412-624-9798; fax: +1-412-624-4846.
E-mail address: pel1@pitt.edu (P.-W. Li).

0378-7753/03/$ – see front matter © 2003 Published by Elsevier Science B.V.
doi:10.1016/S0378-7753(02)00723-1

Nomenclature

A	active area of electrochemical reaction (m^2)
ΔA	unit area (m^2)
C_p	specific heat at constant pressure (J/(kg K))
D	mass diffusion coefficient (m^2/s)
E	electromotive force (EMF) (V)
F	Faraday's constant (96,496.7 C/mol)
ΔG_0	standard state Gibbs free energy change for water, formed from oxygen and hydrogen (J/kg)
H	height of computation domain (m)
i	current density of fuel cell (mA/cm^2)
I	current (A)
k	thermal conductivity (W/(m K))
m	mass flux ($kg/(m^2\ s)$)
M	formula weight (g/mol)
M_m	equivalent weight of membrane (kg/mol)
n_{drag}	electro-osmotic coefficient
p	pressure (Pa)
q	heat flux (W/m^2)
$\dot{q}$	heat source (W/m^3)
R	universal gas constant (8.314 J/(mol K))
S	source term in equations
T	temperature (K)
u	velocity in x-direction (m/s)
v	velocity in y-direction (m/s)
V_{cell}	fuel cell voltage (V)
w	velocity in z-direction (m/s)
x, y, z	Cartesian coordinates (m)
X	mole fraction
Y	mass fraction

Greek letters

β	permeability
δ	thickness of electrode and electrolyte (m)
ε	porosity
η	activation polarization (V)
λ	water content
μ	dynamic viscosity (Pa s)
ρ	density (kg/m^3)
ρ_{dry}	dry density of membrane (kg/m^3)
σ	conductivity $(\Omega\ cm)^{-1}$

Subscripts

a	anode
c	cathode
H_2	hydrogen
H_2O	water vapor
in	at inlet
m	membrane
O_2	oxygen

Superscripts

a	anode
air	air
c	cathode
e	effective
fuel	fuel
H_2	hydrogen
m	membrane
O_2	oxygen
Sat	saturation

heat/mass transfer for a cell stack with all the single fuel cell units subject to investigation would be a difficult task. However, most of the single fuel cell units laminated in a stack can operate under the same conditions if the fuel and oxidant are provided in a parallel style. Therefore, a single PEM fuel cell constructed using the plates illustrated in Fig. 1 will be studied in the present modeling work. This will provide a useful understanding of not only a single fuel cell unit but also a stack of PEM fuel cells.

The flow and heat/mass transfer in a PEM fuel cell have some special features. First of all, there are two flow streams, anodic gas and cathode gas, to be considered in a PEM fuel cell. With the processing of the electrochemical reaction, the species concentration and overall mass flow rate in both the streams experiences associated variation. Therefore, analysis for the fields of flow, temperature and species concentration has to reflect the strong coupling character between the flow streams of the cathode and anode [5,6]. On the one hand, the species and overall mass variation in the two streams of the anode and cathode are affected by the electrochemical reaction proceeding at electrode/electrolyte interfaces. On the other hand, however, the species concentrations and temperature distributions are decisive factors in the electromotive force as expressed by the Nernst equation, which therefore affects the electrical performance of the fuel cell [7,8].

In previous studies, most models focused on one-dimensional (1D) and two-dimensional (2D) flows with transport

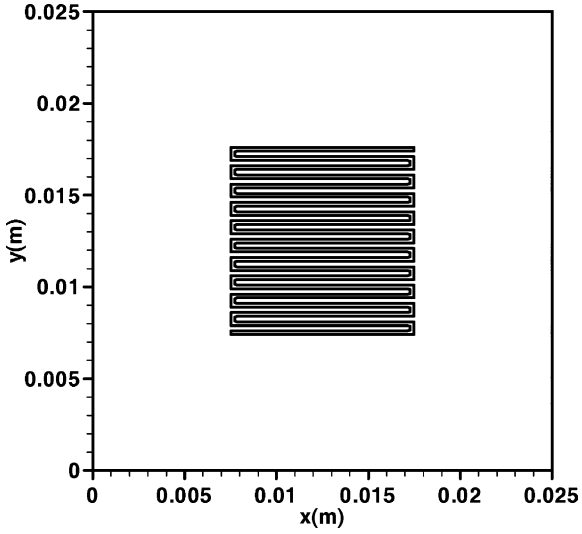

Fig. 1. Copper plate etched with winding gas channels.

of the reactants and products in the flow channels and across the membrane. In particular, those models only treated simple fuel and air channel structures. This allowed the fundamentals of numerical simulation for PEM fuel cells to be established. For example, in the work of Springer et al. [9], they considered a pseudo one-dimensional model in which flows in both fuel and air channels were treated as being well mixed. Fuller and Newman [10] and Nguyen and White [11] developed two-dimensional heat and water transport models that accounted for variation in temperature and membrane hydration conditions along the flow channels. Both of these models assumed a well-mixed concentration in flow channels. However, a fully three-dimensional (3D) solution to the Navier–Stokes equations for the flow channels is important to allow one to account for the effect of the dimensions of the flow channel on the velocity distribution. Also, such a full solution will help one to understand how the mass consumption in the electrochemical reactions affects the momentum transport equations [12].

As a common practical structure, winding fuel and air channels are adopted in PEM fuel cells [13]. Due to the complexity of the flow channels, a three-dimensional model is necessary. This will be one of the focuses of the present study.

2. Model development

From the point of view of numerical analysis, the concern is to predict the details of the flow and heat/mass transfer of two different streams of fuel and air separated by the membrane. However, the heat/mass transfer are strongly coupled between the fuel and air flows through the heat conducting gas channel plate and the mass diffusible membrane. The two channel plates and membrane need to be integrated into one computation domain. Therefore, the computation domain of the x–y-plane includes the whole copper plate as already shown in Fig. 1. The flow directions of fuel and air are arranged as schematically illustrated in Fig. 2.

Governing equations for flow, temperature and mass fractions or concentrations in the PEM fuel cell in three dimensions for the computation domain including the MEA,

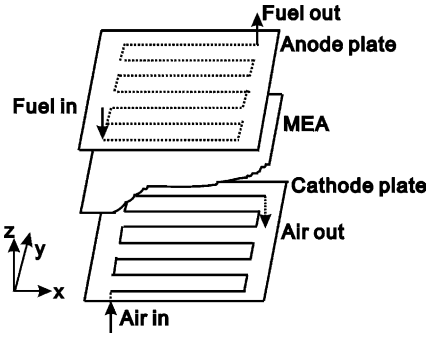

Fig. 2. Flow arrangement for fuel and air gases.

cathode and anode plates (each in thickness of 0.525 mm and both of them have gas channels etched, as illustrated in Fig. 1) are:

$$\frac{\partial(\rho uu)}{\partial x}+\frac{\partial(\rho vu)}{\partial y}+\frac{\partial(\rho wu)}{\partial z} = \frac{\partial}{\partial x}\left(\mu\frac{\partial u}{\partial x}\right)+\frac{\partial}{\partial y}\left(\mu\frac{\partial u}{\partial y}\right)+\frac{\partial}{\partial z}\left(\mu\frac{\partial u}{\partial z}\right)+S_u \quad (5)$$

$$S_u=-\frac{\partial p}{\partial x}+\frac{\partial}{\partial x}\left(\mu\frac{\partial u}{\partial x}\right)+\frac{\partial}{\partial y}\left(\mu\frac{\partial v}{\partial x}\right)+\frac{\partial}{\partial z}\left(\mu\frac{\partial w}{\partial x}\right)-\frac{\mu u}{\beta_x} \quad (6)$$

$$\frac{\partial(\rho uv)}{\partial x}+\frac{\partial(\rho vv)}{\partial y}+\frac{\partial(\rho wv)}{\partial z} = \frac{\partial}{\partial x}\left(\mu\frac{\partial v}{\partial x}\right)+\frac{\partial}{\partial y}\left(\mu\frac{\partial v}{\partial y}\right)+\frac{\partial}{\partial z}\left(\mu\frac{\partial v}{\partial z}\right)+S_v \quad (7)$$

$$S_v=-\frac{\partial p}{\partial y}+\frac{\partial}{\partial x}\left(\mu\frac{\partial u}{\partial y}\right)+\frac{\partial}{\partial y}\left(\mu\frac{\partial v}{\partial y}\right)+\frac{\partial}{\partial z}\left(\mu\frac{\partial w}{\partial y}\right)-\frac{\mu v}{\beta_y} \quad (8)$$

$$\frac{\partial(\rho uw)}{\partial x}+\frac{\partial(\rho vw)}{\partial y}+\frac{\partial(\rho ww)}{\partial z} = \frac{\partial}{\partial x}\left(\mu\frac{\partial w}{\partial x}\right)+\frac{\partial}{\partial y}\left(\mu\frac{\partial w}{\partial y}\right)+\frac{\partial}{\partial z}\left(\mu\frac{\partial w}{\partial z}\right)+S_w \quad (9)$$

$$S_w=-\frac{\partial p}{\partial z}+\frac{\partial}{\partial x}\left(\mu\frac{\partial u}{\partial z}\right)+\frac{\partial}{\partial y}\left(\mu\frac{\partial v}{\partial z}\right)+\frac{\partial}{\partial z}\left(\mu\frac{\partial w}{\partial z}\right)-\frac{\mu w}{\beta_z} \quad (10)$$

$$\frac{\partial(\rho uC_pT)}{\partial x}+\frac{\partial(\rho vC_pT)}{\partial y}+\frac{\partial(\rho wC_pT)}{\partial z} = \frac{\partial}{\partial x}\left(k\frac{\partial T}{\partial x}\right)+\frac{\partial}{\partial y}\left(k\frac{\partial T}{\partial y}\right)+\frac{\partial}{\partial z}\left(k\frac{\partial T}{\partial z}\right)+\dot{q} \quad (11)$$

$$\frac{\partial(\rho uY_j)}{\partial x}+\frac{\partial(\rho vY_j)}{\partial y}+\frac{\partial(\rho wY_j)}{\partial z} = \frac{\partial}{\partial x}\left(\rho D_{j,\mathrm{m}}\frac{\partial Y_j}{\partial x}\right)+\frac{\partial}{\partial y}\left(\rho D_{j,\mathrm{m}}\frac{\partial Y_j}{\partial y}\right)+\frac{\partial}{\partial z}\left(\rho D_{j,\mathrm{m}}\frac{\partial Y_j}{\partial z}\right) \quad (12)$$

Due to the variation of gas species' mass fractions, the local fluid properties could vary significantly. This is also a reflection of the strong coupling of velocities, temperature, and mass fractions, since the determination of the local fluid properties will depend on the local mass fractions and temperatures.

The additional source terms in momentum transport equations, $-\mu u/\beta_x$, $-\mu v/\beta_y$ and $-\mu w/\beta_z$ are only induced in the electrode diffusion layer. The purpose of this is to consider the influence of porous media to flow and mass transfer. It is assumed that the permeability in electrode diffusion layers is isotropic, and thus there is

$$\beta_x=\beta_y=\beta_z \quad (13)$$

For flow and mass fraction equations, only the gas diffusible region is subject to investigation. Treatment through numerical methods [14] will be implemented to induce zero velocities in all of the solid regions in the computation domain.

In the energy conservation equation, the concentration-gradient-induced heat diffusion is very small and thus is neglected [15,16]. The mass fraction of water is monitored at local locations. In case the calculated partial pressure of water vapor is higher than its saturated pressure, it is judged that a condensation of water vapor may happen and that the condensation latent heat will be considered as a heat source at the electrode surface.

Due to the electrochemical reaction and electro-osmotic effect, mass diffusion of water and hydrogen across the membrane will occur. The electrochemical reactants and products must diffuse across electrode layers to reach/leave the reaction site, that is, the interface of the electrolyte and electrodes. The mass diffusion inside the porous electrodes is much weaker than that in the fluid region, so effective diffusivities for mass transport within the electrodes are adopted by inducing a porosity coefficient [17,18]:

$$D^{\mathrm{e}}_{j,\mathrm{m}} = D_{j,\mathrm{m}}\varepsilon^{3/2} \tag{14}$$

2.1. Local current density and determination of mass diffusion fluxes to gas channels

The proton conduction is considered as the electric current. In a plate-type fuel cell, the electric charge passes through the electrolyte layer perpendicularly and is collected by the channel plates. As a function of the local electromotive force, local current density can be calculated by the following correlation:

$$i = \frac{(E - \eta_{\mathrm{act}}) - V_{\mathrm{cell}}}{(\delta_{\mathrm{m}}/\sigma_{\mathrm{m}}) + (\delta_{\mathrm{a}}/\sigma_{\mathrm{a}}) + (\delta_{\mathrm{c}}/\sigma_{\mathrm{c}})} \tag{15}$$

where σ is the electric conductivity of the electrodes or proton conductivity of the electrolyte; δ represents the thickness of the electrodes and electrolyte; and η_{act} is the potential drop due to activation polarization. In the expression of Eq. (4), local partial pressures of gases in the fuel and air channel must be used to calculate the electromotive force E. Because the local partial pressures are obtained from the solution of the governing equations, the convection concentration is thus implicitly considered in E.

By performing a summation or integration of the local current, the total current output from the fuel cell can be obtained:

$$I = \sum(i\,\Delta A) \tag{16}$$

To start a numerical simulation for the fuel cell, the involved total current must be a prescribed electrical parameter, while the cell output voltage V_{cell} and the local current density will be calculated or predicted in the simulation process. Instead of giving the total current over a certain area of electrolyte membrane, the average current density is usually prescribed as a basic given condition.

The activation polarization is a function of the local current density, membrane temperature, and gas pressures, which is expressed as

$$\eta_{\mathrm{act}} = \frac{RT^{\mathrm{m}}(x,y)}{0.5F}\ln\left[\frac{i(x,y)p^{\mathrm{c}}(x,y)}{i_{\mathrm{O_2}}p^{\mathrm{c}}_{\mathrm{O_2}}(x,y)}\right] + \frac{RT^{\mathrm{m}}(x,y)}{1.0F}\ln\left[\frac{i(x,y)p^{\mathrm{a}}(x,y)}{i_{\mathrm{H_2}}p^{\mathrm{a}}_{\mathrm{H_2}}(x,y)}\right] \tag{17}$$

where $i_{\mathrm{O_2}}$ and $i_{\mathrm{H_2}}$ are the constants of exchange current densities, which are property data of the membrane.

With the local current density obtained, the local mass fluxes to the fuel and air channels can be correlated because the electrochemical reaction involving one mole of hydrogen can result in proton flow (electric charge) in two moles. In the air channel, oxygen is consumed, and, as a product of the electrochemical reaction, water is produced. At the same time, the osmotic effect (incorporated through the coefficient of n_{drag}) can cause a certain number of water molecules to be dragged from the anode side of the air channel through the electrolyte membrane. Moreover, water might diffuse in between the anode and cathode side through the electrolyte membrane. Considering these above mass transfer processes, the oxygen flux and overall water flux on the cathode side is formed as

$$m^{\mathrm{c}}_{\mathrm{O_2}} = M_{\mathrm{O_2}}\frac{i}{4F} \tag{18}$$

$$m^{\mathrm{c}}_{\mathrm{H_2O}} = -\left[M_{\mathrm{H_2O}}\frac{i}{2F} + M_{\mathrm{H_2O}}n_{\mathrm{drag}}\frac{i}{F} - D^{\mathrm{m}}_{\mathrm{H_2O}}\frac{\rho_{\mathrm{dry}}}{M_{\mathrm{m}}}\frac{(\lambda^{\mathrm{c}}_{\mathrm{H_2O}} - \lambda^{\mathrm{a}}_{\mathrm{H_2O}})}{\delta_{\mathrm{m}}}\right] \tag{19}$$

In the fuel channel, hydrogen is consumed and the balance of water is due to the osmotic effect and diffusion effect:

$$m^{\mathrm{a}}_{\mathrm{H_2}} = -M_{\mathrm{H_2}}\frac{i}{2F} \tag{20}$$

$$m^{\mathrm{a}}_{\mathrm{H_2O}} = -\left[M_{\mathrm{H_2O}}n_{\mathrm{drag}}\frac{i}{F} + D^{\mathrm{m}}_{\mathrm{H_2O}}\frac{\rho_{\mathrm{dry}}}{M_{\mathrm{m}}}\frac{(\lambda^{\mathrm{c}}_{\mathrm{H_2O}} - \lambda^{\mathrm{a}}_{\mathrm{H_2O}})}{\delta_{\mathrm{m}}}\right] \tag{21}$$

where M is the molecular weight, and $\lambda^{\mathrm{a}}_{\mathrm{H_2O}}$ and $\lambda^{\mathrm{c}}_{\mathrm{H_2O}}$ are the water content of the membrane at the interfaces of the anode and cathode sides. According to Springer et al. [9], water content can be calculated from the activity of water by the correlation:

$$\lambda = \begin{cases} 0.043 + 17.81\alpha - 39.85\alpha^2 + 36.0\alpha^3, & \text{for } 0 < \alpha \le 1 \\ 14.0 + 1.4(\alpha - 1.0), & \text{for } 1 < \alpha \le 3 \end{cases} \tag{22}$$

where α is given as

$$\alpha = \frac{X_{\mathrm{H_2O}}p(x,y)}{p^{\mathrm{Sat}}_{\mathrm{H_2O}}} \tag{23}$$

in which X is the mole fraction.

In this model, we did not consider the possibility of large excesses of liquid water in the flow channels or within the electrodes. For the continuity equations, no distinction was made between water gas and liquid molecules. It is assumed that the vapor and membrane phases are in phase equilibrium. The activity of water in the vapor phase on anode side is set equal to the activity of water in the membrane [19].

The membrane properties of proton conductivity, σ_m, water diffusivity, and osmotic coefficient, n_{drag}, all depend on the water content of the membrane. Empirical expressions for the Nafion membrane were recommended in different sources [20]; however, they are mostly based on the correlations by Springer et al. [9]:

$$D^{m}_{H_2O} = D_\lambda \exp\left(2416\left(\frac{1}{303} - \frac{1}{T}\right)\right) \tag{24}$$

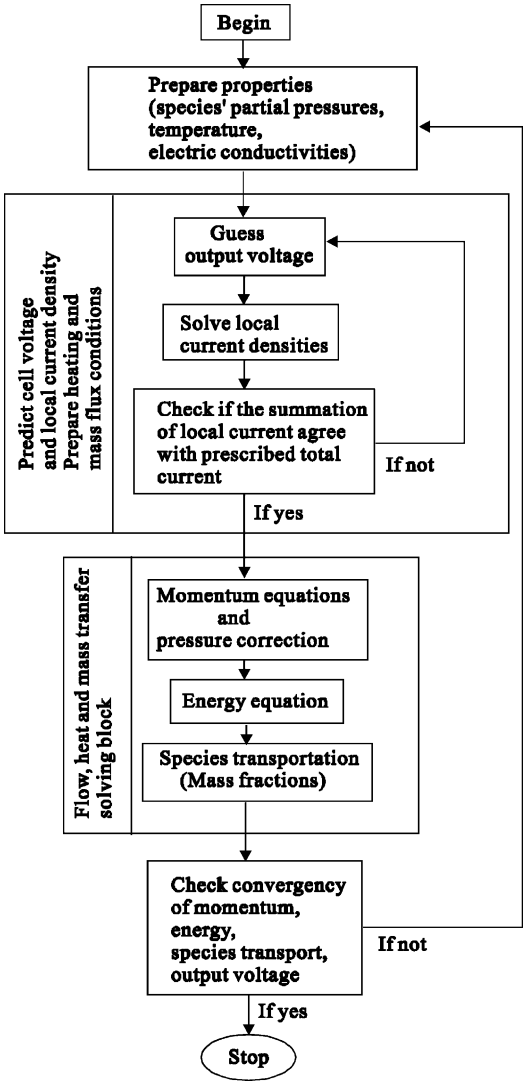

Fig. 3. Flow chart of the computation procedure.

where

$$D_\lambda = \begin{cases} 10^{-10}, & \text{for } \lambda < 2 \\ 10^{-10}(1 + 2(\lambda - 2)), & \text{for } 2 \le \lambda \le 3 \\ 10^{-10}(3 - 1.67(\lambda - 3)), & \text{for } 3 < \lambda < 4.5 \\ 1.25 \times 10^{-10}, & \text{for } \lambda \ge 4.5 \end{cases} \tag{25}$$

$$\sigma_m = (0.00514\lambda - 0.00326)\exp\left(1268\left(\frac{1}{303} - \frac{1}{T}\right)\right) \times 10^2 \tag{26}$$

$$n_{drag} = 0.0029\lambda^2 + 0.05\lambda - (3.4 \times 10^{-19}) \tag{27}$$

It may be a disadvantage that there has been no application of these equations for a temperature level lower than 30 °C.

The average current density, initial gas species and mass fractions are all specified as known conditions of the numerical simulation. The fuel and air flow rates fed to the fuel cell can be determined through the following two equations:

$$G^{fuel}_{in} = \frac{iA}{2F}\frac{RT^{fuel}_{in}}{P^{fuel}_{in}X^{H_2}_{in}} \tag{28}$$

$$G^{air}_{in} = \frac{iA}{4F}\frac{RT^{air}_{in}}{P^{air}_{in}X^{O_2}_{in}} \tag{29}$$

Table 1
Fuel and air conditions[a]

	Mole fraction	
Air (1.1×10^5 Pa)		
Oxygen	0.18	
Nitrogen	0.81	
Water vapor	0.01	
Fuel (1.1×10^5 Pa)		
Hydrogen	0.80[b]	0.60[c]
Water vapor	0.20[b]	0.40[c]

[a] Temperature: 85 °C.
[b] Case 1.
[c] Case 2.

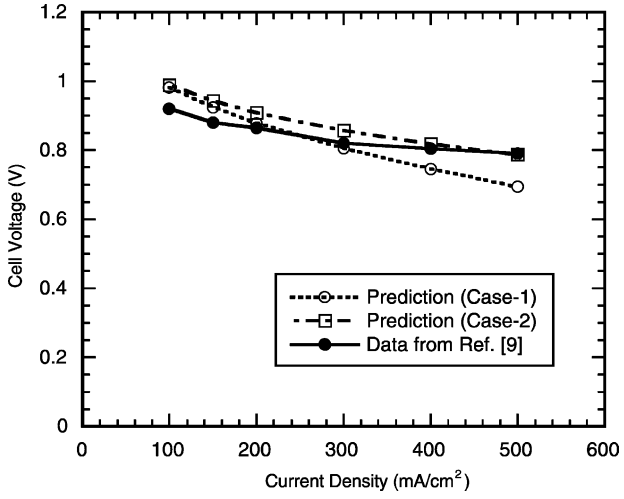

Fig. 4. Cell voltage vs. current density.

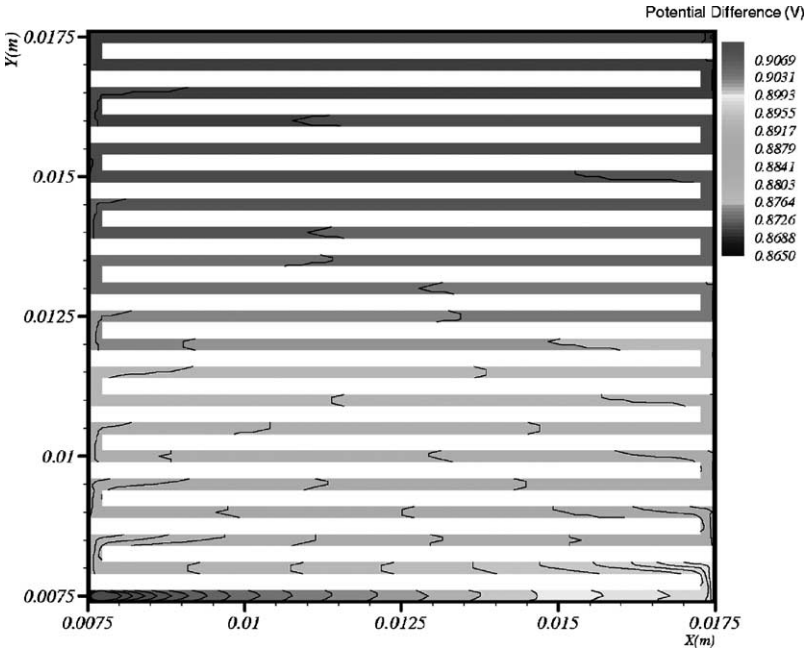

Fig. 5. Local distribution of potential difference $(E - \eta_{act})$.

Other related parameters and property data for the Nafion electrolyte membrane to be used in this work are available in the literature [12]. These are:

- thickness of dry membrane (Nafion 112:2mil) (μm): 51;
- density of dry membrane (g/cm^3): 1.84;
- equivalent weight of membrane (g/mol): 1100;
- exchange current density (A/m^2): $i_{H_2} = 100.0$ (anode), $i_{O_2} = 1000.0$ (cathode);
- permeability of porous electrode (m^2): $\beta = 2.3 \times 10^9$;
- porosity of porous electrode: $\varepsilon = 0.4$.

2.2. Numerical treatment and computation procedures

A non-uniform mesh arrangement is deployed in the computation domain, in which the gas channels and membrane regions are allocated a finer mesh. The SIMPLE algorithm [14] is adopted to link the velocity and pressure. Flow, temperature and mass fractions for each species are solved in each iteration step.

Considering the situation of one fuel cell unit in a PEM fuel cell stack, its anode plate contacts the cathode plate of the neighboring unit while its cathode plate contacts the

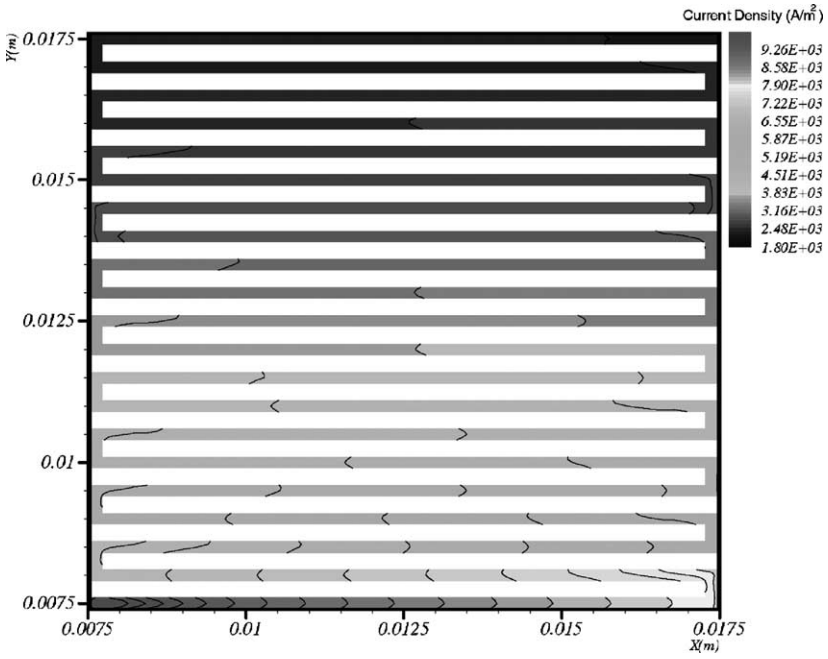

Fig. 6. Local distribution of current density.

anode plate of the other-side neighboring unit. Suppose that every fuel cell unit operates at the same conditions. Then it is plausible to assume that the outside surface temperature of cathode and anode plates must comply to the condition of a consecutive heat flux, that is:

$$q(x,y)|_{z=0} = q(x,y)|_{z=H} \tag{30}$$

The computational outflow boundary conditions of temperature and velocities for both flows of fuel and air are treated based on the methods from [21,22].

The iterative computation follows the flow chart as shown in Fig. 3, and can be described concisely as follows:

(1) The latest available mass fractions and pressures are used to calculate the local current densities and

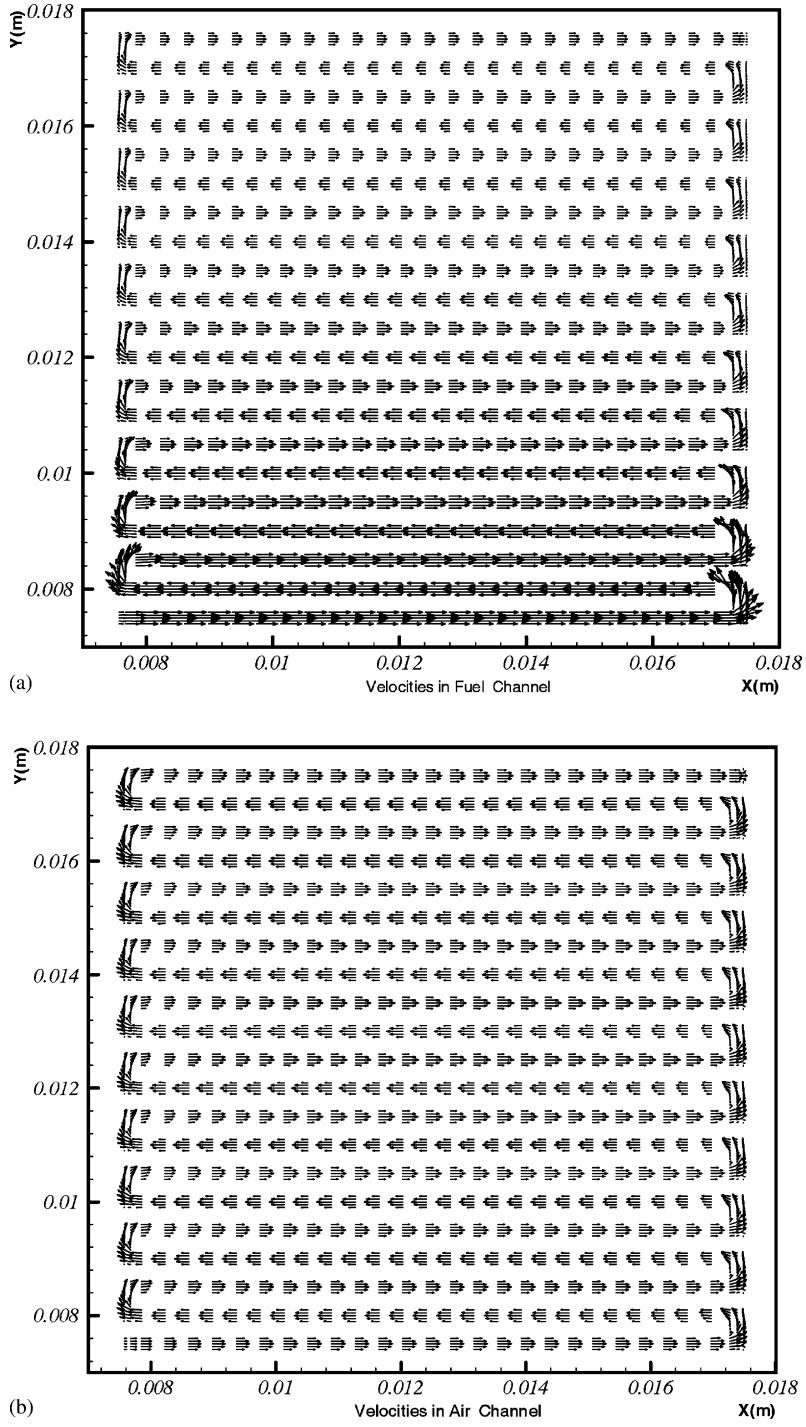

Fig. 7. Velocity vectors in the air and fuel channels at the half channel height: (a) fuel; (b) air.

therefore the related heat generation, as well as the mass fluxes perpendicular to the flow channels at the membrane surfaces. An inner iteration in this step has to be conducted to guess and find a proper cell voltage, so that the integrated total current from the local current density satisfactorily agrees with the prescribed total current.

(2) Equations of velocity, temperature and mass fractions are solved in series.

(3) The convergence of both electrical results and the results of velocity, temperature and mass fractions are checked. In case no convergence is attained, additional computational iteration will be necessary, thereby returning to the Step (1).

3. Application computation

The investigated fuel cell unit has dimensions marked in Fig. 1. Operating conditions are listed in Table 1. With these prescribed temperatures and species' mass fractions in fuel and air, the fuel cell electrical performance and local details

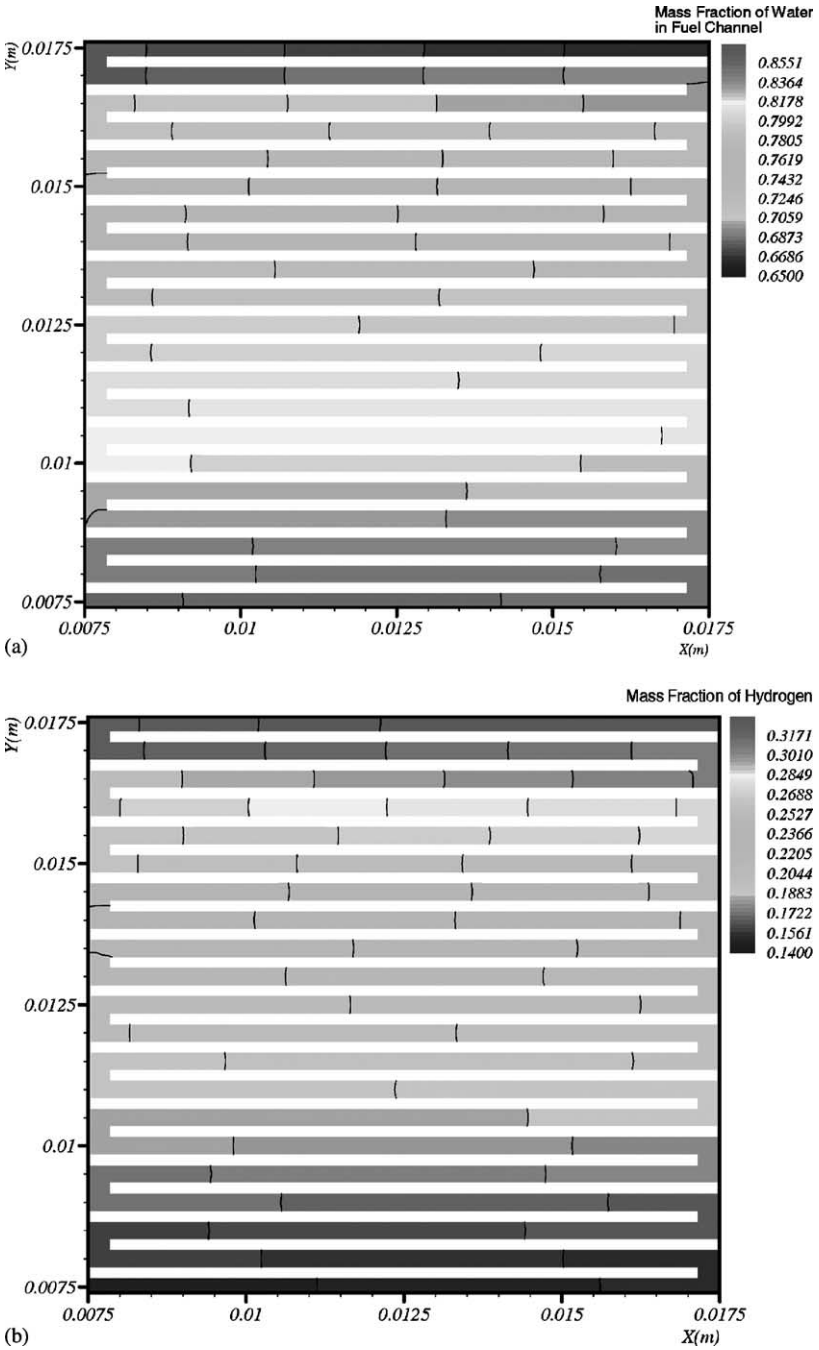

Fig. 8. Mass fraction variation of gases in the fuel channel: (a) water; (b) hydrogen.

of the velocity, mass fraction, and temperature are obtained and will be presented in this section.

3.1. Electrical performance

Fig. 4 shows the fuel cell terminal voltage against current density obtained through numerical calculations for series of cell current densities. The *V–I* data of a single cell from the work of Springer et al. [9] in the similar membrane conditions to the present work are plotted for reference, of which the operation temperature was 80 °C and Nafion 117 membrane thickness was 50 μm. The cell voltages were found in the level quite approximate. However, the present fuel and air channel structure is quite different from that of Springer et al. [9]. This can be the reason that in the *V–I* curves there are some differences.

Prediction computation was done for two different cases in different fuel quality or humidity. A significant effect of humidity to the cell voltage can be seen when current density becomes larger as illustrated by the predicted curves of

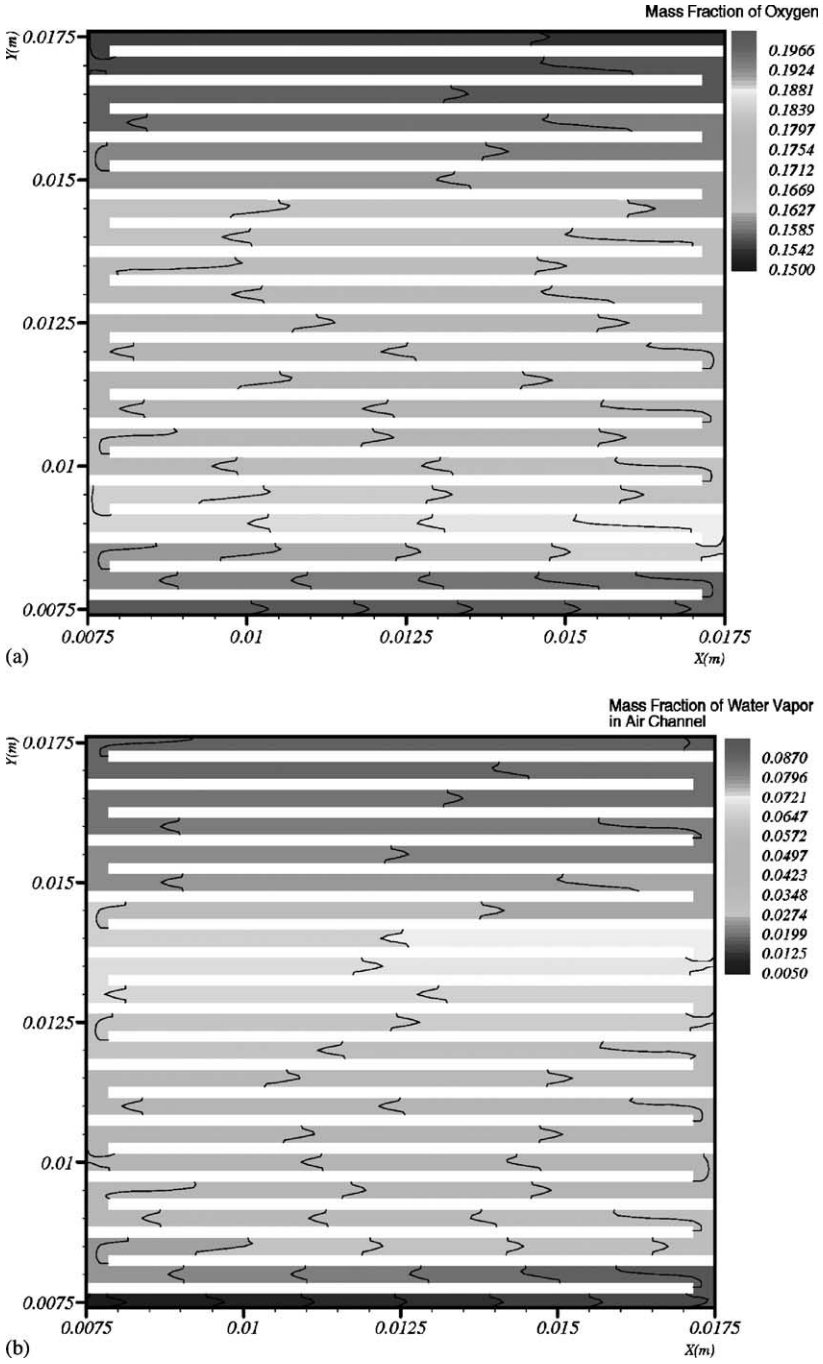

Fig. 9. Distribution of the gas species' mass fractions in the air channel: (a) oxygen; (b) water; (c) nitrogen.

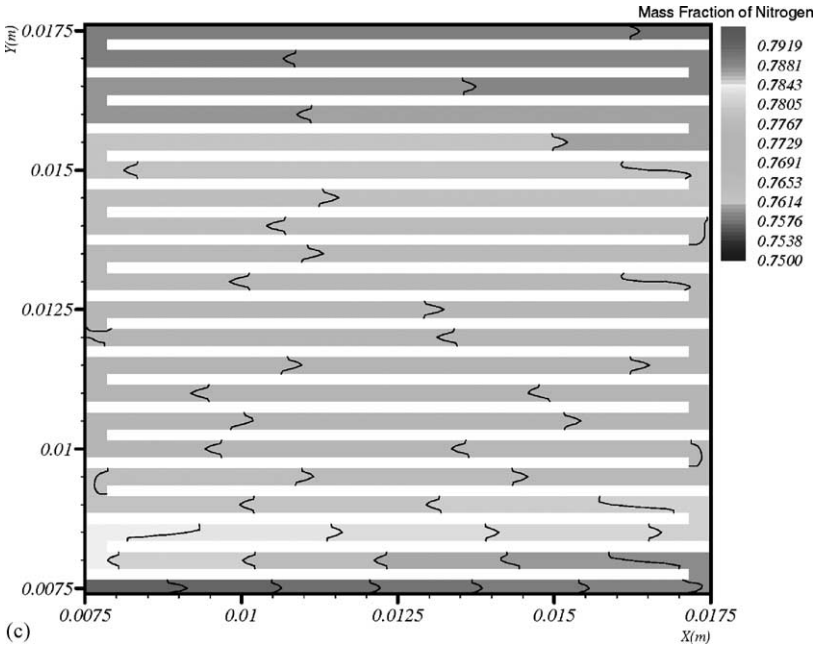

Fig. 9. (*Continued*).

voltage versus current density. When the mole fraction of water vapor increases from 20 to 40%, the cell voltage increment can be as large as 0.1 V at the current density of 500 mA/cm^2.

The local distribution of cell potentials $(E - \eta_{act})$ at a current density of 400 mA/cm^2 and fuel composition in Case 2 is given in Fig. 5. A high potential can be found at the upstream region of fuel and air. It then decreases along the stream, and the decrement at the upstream region is faster than that at downstream region. The corresponding local distribution of current density is given in Fig. 6. A dramatic variation or decrease of the local current density along the stream could be observed. At the end of the flow stream the electrochemical reaction is quite weak.

3.2. Velocity fields

The velocity vectors in x–y-plane at the half height of air and fuel channels are shown in Fig. 7 for the condition of a current density of 400 mA/cm^2 and fuel composition of Case 2. In the fuel gas channel, velocities decrease along the streamwise direction. This reflects the depletion of mass in the fuel channel, which includes the consumption of hydrogen and loss of water due to the osmotic effect that drags water from the anode to the cathode in the electrochemical reaction process. Although there is water diffusion from the cathode side to the anode side, it is relatively weak and cannot compensate for the water loss from the osmotic effect.

In the air channel, consumption of oxygen accompanies the production of water in the electrochemical reaction. Contrast to the fuel/anode channel, the air/cathode channel has a net income of water that is induced collectively from the electrochemical reaction, osmotic drag effect and diffusion effect. However, compared to the overall mole flow rate (including oxygen, nitrogen and water) in the air channel, this water is still only a small proportion. This is the reason that we could not see any significant increase in the velocity in air channel.

3.3. Fields of mass fraction

The local distributions of the species' mass fractions in the fuel channel for the forgoing discussed case are shown in Fig. 8. It is known that both hydrogen and water vapor in the fuel channel are consumed or transferred to the cathode side. As a collective result of the osmotic effect and mass diffusion through the membrane, the mass fraction of water vapor in the fuel channel decreases along the streamwise direction. Interestingly, it can also be seen that the hydrogen mass fraction has a relative increment along the stream. Examining the osmotic drag coefficient, one can find that its value may range from 0.2 to 0.9 depending on the local water content of membrane; therefore, the electrochemical reaction using 1 mol of hydrogen might cause 0.4–1.8 mol of water to be dragged to the cathode side. This is a dramatic decrease of the mass fraction of water in the fuel channel, and thus the mass fraction of hydrogen relatively increases, although the hydrogen has a net reduction due to the electrochemical reaction. From this observation, it is believed that water loss on the fuel side is serious and the probability of water condensation in the fuel channel is very low.

In the air channel, oxygen is consumed and water is generated due to the electrochemical reaction and osmotic effect. These variations can be observed in Fig. 9, which

displays the local distributions of the mass fractions for each of the species along the streamwise direction. Oxygen is consumed, and thus its mass fraction decreases along the streamwise direction. As a product of the electrochemical reaction, water is generated in the air channel. In addition, the osmotic effect in the electrochemical reaction drags water from the anode to cathode, although water inversely diffuses from the cathode to anode side. However, the net result is that water increases in the air channel, which can be seen in Fig. 9b. Because the nitrogen and oxygen are in rather high proportions, the partial pressure of the water vapor is relatively low, and thus there is no condensation of water under the investigated temperature and concentration conditions.

Fig. 9c is the mass fraction variation of nitrogen. Although the quantity of nitrogen in air has no variation in concentration, its mass fraction decreases because water is produced in air channel.

A careful examination of Figs. 8 and 9 may find that the mass diffusion in the fuel and air channels exhibits some differences. In the fuel channel, the contour line is rather flat normal to flow direction, which indicates that the diffusion of hydrogen and water vapor is rather strong, and the mass fraction is relatively uniform in the cross section normal to the flow stream. However, in the air channel, the contour profile is mostly in a parabolic shape. This is a reflection that the diffusion of oxygen, nitrogen and water vapor is weak compared to that of the gases in the fuel channel, which also indicates the three-dimensional effect of the transportation problem for the cathode side.

4. Concluding remarks

A three-dimensional numerical model simulating the performance of a proton exchange membrane (PEM) fuel cell with complicated gas channels is developed to show the strong coupling of the flow and heat/mass transfer with the electrochemical reaction. The numerical model is applied to simulate a single PEM fuel cell unit. The fields of flow, mass fraction, and local electromotive force were obtained and discussed. The simulation results show that the fuel gas humidity has a significant effect on the output voltage of the fuel cell. It was also found that due to the electrochemical reaction and osmotic effects, the air channel has an increasing mass fraction of water, and therefore, the oxygen mass fraction or partial pressure is decreased. While high humidity of the fuel gas is desirable, excessive increase of water in the air channel could reduce the cell performance. An optimized condition of humidity might exist, however, but heavy computations are necessary. It was also found that mass diffusion is strong in the fuel channel but is rather weak in the air channel. To facilitate a better diffusion of oxygen in the air channel, modification of the air channel and flow arrangement might be ways to improve the PEM fuel cell performance.

References

[1] S. Srinivasan, R. Mosdale, P. Stevens, C. Yang, Annu. Rev. Energy Environ. 24 (1999) 281–328.
[2] T. Susai, A. Kawakami, A. Hamada, Y. Miyake, Y. Azegami, J. Power Sources 92 (2001) 131–138.
[3] C. Yang, P. Costamagna, S. Srinivasan, J. Benziger, A.B. Bocarsly, J. Power Sources 103 (2001) 1–9.
[4] C. Wallmark, P. Alvfors, J. Power Sources 106 (2002) 83–92.
[5] G. Maggio, V. Recupero, L. Pino, J. Power Sources 101 (2001) 275–286.
[6] A.A. Kulikovsky, Electrochem. Commun. 3 (2001) 460–466.
[7] I.M. Hsing, P. Futerko, Chem. Eng. Sci. 55 (2000) 4209–4218.
[8] R.F. Mann, J.C. Amphlett, M.A.I. Hooper, H.M. Jensen, B.A. Peppley, P.R. Roberge, J. Power Sources 86 (2000) 173–180.
[9] T.E. Springer, T.A. Zawadzinski, S. Gottesfeld, J. Electrochem. Soc. 138 (8) (1991) 2334–2342.
[10] T.F. Fuller, J. Newman, J. Electrochem. Soc. 140 (1993) 1218–1225.
[11] T.V. Nguyen, R.E. White, J. Electrochem. Soc. 140 (1993) 2178–2186.
[12] S. Shimpalee, S. Dutta, Numer. Heat Transfer A 38 (2000) 111–128.
[13] H. Dohle, A.A. Kornyshev, A.A. Kulikovsky, J. Mergel, D. Stolten, Electrochem. Commun. 3 (2000) 73–80.
[14] S.V. Patankar, Numerical Heat Transfer and Fluid Flow, McGraw-Hill, New York, 1980.
[15] R.B. Bird, W.E. Stewart, E.N. Lightfoot, Transport Phenomena, Wiley, New York, 1960.
[16] F.A. Williams, Combustion Theory, Benjamin/Cummings, Menlo Park, CA, 1985.
[17] D.M. Bernardi, M.W. Verbrugge, AIChE J. 37 (1991) 1151.
[18] D.M. Bernardi, M.W. Verbrugge, J. Electrochem. Soc. 139 (1992) 2477.
[19] P. Futerko, I.M. Hsing, J. Electrochem. Soc. 146 (1999) 2049.
[20] S.C. Yeo, A. Eisenberg, J. Appl. Polym. Sci. 21 (1977) 875–898.
[21] P.-W. Li, W.Q. Tao, Warme und Stoffubertragung 29 (1994) 463–470.
[22] M.H. Kobayashi, J.C.F. Pereira, M.M. Sousa, Int. J. Numer. Methods Fluids 16 (1993) 403–419.